TABLE 5 | Troubleshooting table (continued).

Step	Problem	Possible reason	Solution
	No differentiation or too-low efficiency in differentiation	Improper cell density	Perform induction of differentiation in an appropriate cell density according to the protocol
20A(iv), 20C(ii)	The signal for the specific cell type cannot be detected in cultured cells on a gelatin-coated coverslip	Prolonged culturing	Do not culture cells on a gelatin-coated coverslip until they reach 100% confluency or specific cell types will be lost

● **TIMING**

Step 1, preparation of adult human dermal fibroblasts or bone marrow stromal cells: 4 h–3 weeks
Step 1A, preparation of adult human dermal fibroblasts: 4 h–3 weeks
Step 1A(i–vii), thawing and culturing: 2–3 weeks
Step 1A(viii–xii), passaging: 1–2 h
Step 1A(xiii–xviii), preparation for FACS: 1 d
Box 1, making frozen stock for mesenchymal cells: 1 h
Box 2, selecting serum by lot check: 2 weeks
Step 1B, preparation of fresh bone marrow–derived mononuclear cells: 4 h
Steps 2–9, isolation of Muse cells by FACS: 4–6 h
Step 10, M-cluster formation in suspension culture: 7–10 d
Step 10A, single-cell suspension culture: 7–10 d
Step 10B, MC culture: 7–10 d
Steps 11–17, adherent culture: 7–10 d
Step 18, evaluation of Muse cells in M-clusters: 1.5 h–2 d
Step 18A, detection of ALP activity: 1.5 h
Step 18B, immunocytochemistry against pluripotency markers: 2 d
Step 19, evaluation of the differentiation capacity of Muse cells: 1–3 weeks
Step 19A, spontaneous differentiation on a gelatin-coated coverslip: 1–2 weeks
Step 19B, dissociation of M-clusters for induced differentiation of Muse cells into mesodermal-, endodermal- and ectodermal-lineage cells: 1 h
Step 19C, induced differentiation of Muse cells into mesodermal-, ectodermal- and endodermal-lineage cells: 2–3 weeks
Step 19C(ii–vi), osteocyte induction: 2–3 weeks
Step 19C(vii–ix), adipocyte induction: 2–3 weeks
Step 19C(x–xi), hepatocyte induction: 2 weeks
Step 19C(xii–xvi), neural induction: 3 weeks
Step 20, evaluation of cell differentiation: 5 h–2 d
Step 20A, immunocytochemical analysis of the differentiated cells: 2 d
Step 20B, immunocytochemical analysis of the sphere cells: 2 d
Step 20C, RT-PCR: 5 h

ANTICIPATED RESULTS

In the case of isolation of Muse cells from cultured mesenchymal cell populations that can be purchased commercially, adult human BMSCs and dermal fibroblasts should be cultured in the appropriate culture conditions described in the PROCEDURE. Healthy MSCs have long, thin cell bodies with a large nucleus, usually referred to as 'fibroblast-like morphology', and MSCs cultured in a 90-mm tissue culture dish generate 1.0×10^6 BMSCs, 2.0×10^6 NHDFs and 2.1×10^6 HDFas at 100% confluency (**Fig. 3**). In contrast, mononuclear cells derived from fresh bone marrow are another cell source for Muse cells. According to the brochure accompanying the commercial bone marrow preparation, the number of mononuclear cells elicited from 10 ml of fresh bone marrow is calculated as $0.2–1.7 \times 10^8$ cells, but it actually depends on the freshness of the bone marrow aspirates. For example, when we purchased bone marrow from ALLCELLS, which is imported from the United States to Japan and typically takes 5–7 d to arrive, the number of mononuclear cells elicited from the bone marrow aspirate was as low as about $2.0–5.0 \times 10^6$ cells, and sometimes no cells could be collected. We strongly recommend isolating mononuclear cells as soon as possible after aspiration of the bone marrow.

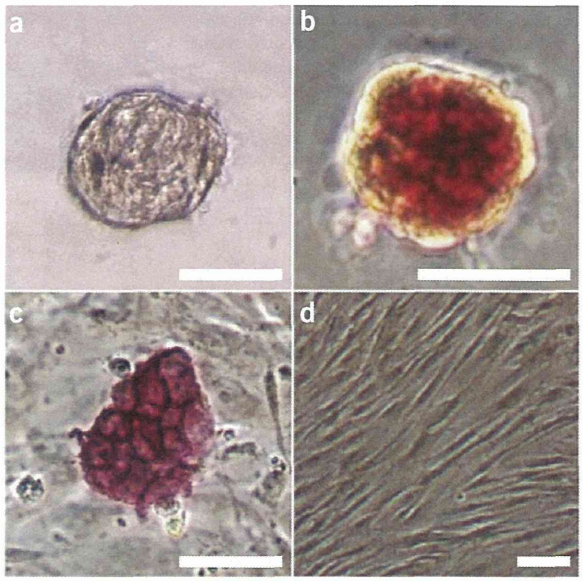

Figure 5 | Characterization of M-clusters. (**a**) Phase-contrast image of an M-cluster. (**b–d**) The result of the ALP reaction; the M-cluster (**b**) and mouse ES cells (**c**) are positive for the ALP reaction, whereas NHDFs (**d**) are negative. Scale bars, 50 μm (**a–c**), 100 μm (**d**).

Muse cells can be purified from the mesenchymal cell populations such as adult human BMSCs, dermal fibroblasts and the mononuclear cell population of fresh bone marrow by FACS using the antibody against the specific cell surface marker SSEA-3 (**Fig. 4**). The percentage of SSEA-3$^+$ cells among these cell populations is dependent on the cell sources: it is <1% in adult human cultured BMSCs, 2–3% in adult human cultured fibroblasts and 0.003–0.004% in mononuclear cells directly isolated from fresh bone marrow. Muse cells have telomerase activity as low as that of naive fibroblasts or BMSCs (**Supplementary Fig. 1**), suggesting low tumorigenicity of Muse cells. After SSEA-3$^+$ cells are isolated, they can be cultured in a single-cell suspension culture or an MC culture. About half (40–60%) of the Muse cells form M-clusters, whose diameters are >25 μm and which resemble embryoid bodies generated from human ES cells, have ALP activity similar to that of other pluripotent cells (**Fig. 5**) and contain the cells positive for pluripotency markers such as Nanog, Oct3/4 and Sox2 in addition to SSEA-3 (as shown by immunocytochemical analysis and RT-PCR (**Fig. 6**)). The growth curve of Muse cells in M-cluster formation shows the limitation of proliferative activity of Muse cells in a single-cell suspension culture (**Supplementary Fig. 2**). The proportion of M-cluster–forming activity is dependent on the viability of cells and is usually 45–65% in our laboratory. In contrast, SSEA-3$^-$ and/or CD105$^-$ cells did not form any clusters after single-cell suspension culture or MC culture. After expansion of M-clusters in adherent culture, second-generation M-cluster can be formed from the M-cluster-derived adherent culture–expanded cells, and the proportion of second-generation M-cluster formation is 48.0 ± 5.8% (fibroblasts) (mean ± s.d.) or 40.3 ± 9.1% (BMSCs). Alternatively, Muse cells can be isolated by FACS sorting with anti–SSEA-3 antibody, and the percentage of SSEA-3$^+$ cells is 45.0 ± 3.2% (fibroblasts). This SSEA-3$^+$ percentage is similar to the proportion of M-cluster-forming cells after adherent culture presented above, suggesting that SSEA-3$^+$ Muse cells have M-cluster-forming activity.

Differentiation of Muse cells can be confirmed by two methods: a spontaneous differentiation assay in which they are cultured on the gelatin-coated coverslip or induced differentiation of Muse cells into mesodermal-, endodermal- and ectodermal-lineage cells. After culturing on a gelatin-coated coverslip with 10% (vol/vol) FBS in α-MEM, Muse cells spontaneously differentiate into cells representative of all three germ layers, including cells positive for neuro-filament (marker for neuronal cells, ectodermal lineage), SMA (smooth muscle, mesodermal lineage), α-fetoprotein (hepatocyte, endodermal lineage), cytokeratin-7 (biliary duct, endodermal lineage) and desmin (muscle, mesodermal lineage) (**Fig. 7a–d**). RT-PCR demonstrates the expression

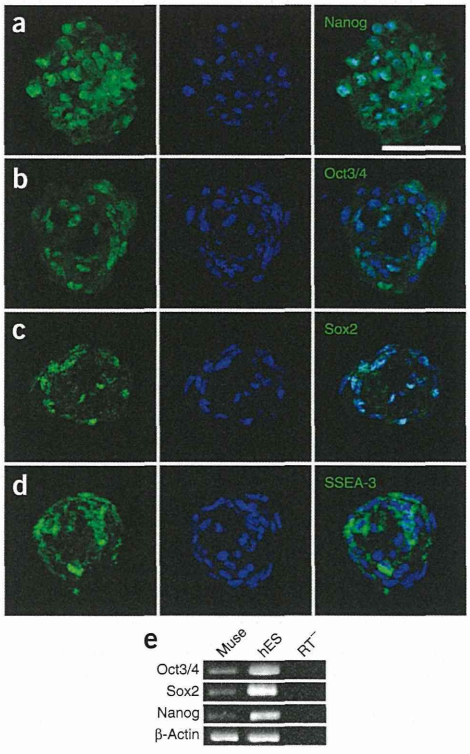

Figure 6 | Expression of pluripotency markers in M-clusters. (**a–d**) Immunocytochemical analysis showing cells in an M-cluster expressing pluripotency markers (green) such as Nanog (**a**), Oct3/4 (**b**), Sox2 (**c**) and SSEA-3 (**d**); nuclei are also visualized (blue). (**e**) mRNA expression of pluripotency markers. Human ES cells are used as a positive control. Scale bar, 50 μm. Samples treated without a reverse-transcription reaction (RT$^-$) are used as a negative control. Panels **a**,**b**,**e** are modified from Kuroda *et al.*[39], Wakao *et al.*[40] and Kuroda *et al.*[39], respectively.

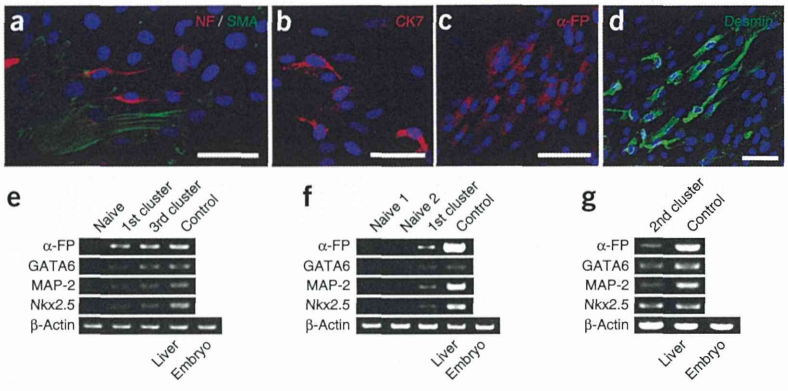

Figure 7 | Spontaneous differentiation of Muse cells on a gelatin-coated coverslip. (**a–d**) Immunocytochemistry against markers for specific cell types; M-cluster–derived cells cultured on gelatin-coated coverslips are positive for neurofilament NF and SMA (**a**), cytokeratin-7 (CK7) (**b**), α-fetoprotein (α-FP) (**c**) and desmin (**d**). (**e–g**) Expression of mRNA for cell lineage markers. M-cluster-derived cells cultured on the gelatin-coated coverslip express mRNA for α-FP, GATA6, MAP-2 and Nkx2.5 (**e**, cells from M-clusters derived from adult human dermal fibroblasts; (**f**,**g**) cells from M-clusters derived from a mononucleated cell of human fresh bone marrow). Human fetal liver (liver) was used as a positive control for α-FP, and whole human embryo (embryo) was used as a positive control for GATA6, MAP-2 and Nkx2.5. Scale bars, 50 μm. Panels **a**,**g** are modified from Wakao *et al.*[40] and Kuroda *et al.*[39], respectively.

of α-fetoprotein, GATA6 (endodermal lineage), MAP-2 (ectodermal lineage) and Nkx2.5 (mesodermal lineage) (**Fig. 7e–g**). Muse cells without induction of differentiation do not express any of the differentiation markers mentioned above, as shown by immunocytochemical analysis and RT-PCR (**Supplementary Fig. 3**).

The self-renewal property of Muse cells can be confirmed by cycle culture consisting of suspension culture–adherent culture–suspension culture. M-cluster in the third generation created by this cycle-culture method also has the same differentiation ability as that observed in the first generation (**Fig. 7e**), indicating the self-renewal property of Muse cells. Muse cells can differentiate into mesodermal-, endodermal- and ectodermal-lineage cells under the directed method. For example, Muse cells give rise to osteocalcin-positive osteocytes (**Fig. 8**) and adipocytes (mesodermal lineage) that are detected as cells containing lipid droplets inside the cytoplasm (**Fig. 8b**), and which are positive for oil red staining (**Fig. 8c**). These cells are representative of the mesodermal lineage. Hepatocytes (endodermal lineage) that express α-fetoprotein and human albumin are able to be produced from Muse cells after culturing with 10% (vol/vol) serum-containing medium supplemented with several hormones and trophic factors, including dexamethasone, HGF and FGF-4 (**Fig. 8d,i**). In the suspension culture system containing bFGF and EGF in a serum-free medium, Muse cells can also give rise to neural progenitor cells, which are positive for nestin (**Fig. 8e**), musashi-1 (**Fig. 8f**) and NeuroD (**Fig. 8g**) (ectodermal lineage). These neural progenitor cells differentiate into MAP-2$^+$ neurons upon treatment with bFGF and BDNF in adherent culture (**Fig. 8h**). These procedures confirm Muse cells' capacity for differentiation and self-renewal.

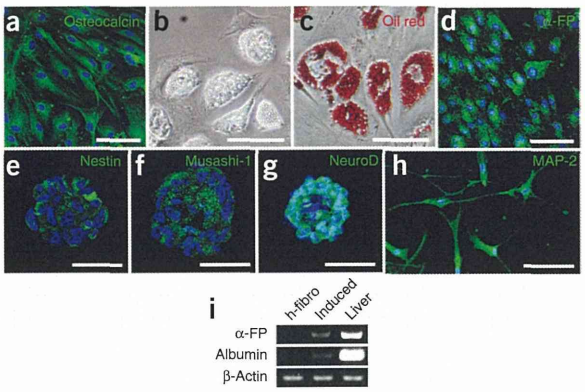

Figure 8 | Induced differentiation of Muse cells into mesodermal-, endodermal- and ectodermal-lineage cells. (**a–h**) Immunocytochemical analysis of differentiated cells. (**a**) After osteocyte induction, the cells positive for osteocalcin are detected. Adipocyte induction generates cells with lipid droplets (**b**) that are positive for oil red staining (**c**). (**d**) Hepatocyte induction generates cells positive for α-fetoprotein (α-FP). (**e–g**) After neural induction, the cells form spheres resembling neurospheres positive for the neural progenitor markers (green) Nestin (**e**), Musashi-1 (**f**) and NeuroD (**g**). (**h**) This neurosphere-like sphere gives rise to MAP-2$^+$ neurons after treatment with trophic factors. (**i**) mRNA expression in differentiated hepatocytes. M-cluster–derived cells (induced) can differentiate into cells expressing α-FP and human albumin mRNA, whereas naive adult human fibroblasts (h-fibro) do not express both mRNAs. Human fetal liver (liver) was used as a positive control. Scale bars, 50 μm (**a**,**d–h**), 20 μm (**b**,**c**).

Note: Supplementary information is available in the online version of the paper.

ACKNOWLEDGMENTS This work was supported by the Japan New Energy and Industrial Technology Development Organization. Antibodies against Oct3/4 were a gift from H. Hamada (Osaka University).

AUTHOR CONTRIBUTIONS Y.K., S.W., M.K. and M.D. contributed to the development of the methodology, Y.K., S.W., M.K., M.N. and M.D. performed the experiments and all the authors prepared the figures. M.K. and M.D. contributed to the description of the protocols.

COMPETING FINANCIAL INTERESTS The authors declare competing financial interests: details are available in the online version of the paper.

1. Gage, F.H. Mammalian neural stem cells. *Science* **287**, 1433–1438 (2000).
2. Weissman, I.L. & Shizuru, J.A. The origins of the identification and isolation of hematopoietic stem cells, and their capability to induce donor-specific transplantation tolerance and treat autoimmune diseases. *Blood* **112**, 3543–3553 (2008).
3. Kitada, M. & Dezawa, M. Induction system of neural and muscle lineage cells from bone marrow stromal cells; a new strategy for tissue reconstruction in degenerative diseases. *Histol. Histopathol.* **24**, 631–642 (2009).
4. Kuroda, Y., Kitada, M., Wakao, S. & Dezawa, M. Bone marrow mesenchymal cells: how do they contribute to tissue repair and are they really stem cells? *Arch. Immunol. Ther. Exp. (Warsz)* **59**, 369–378 (2011).
5. Pittenger, M.F. *et al.* Multilineage potential of adult human mesenchymal stem cells. *Science* **284**, 143–147 (1999).
6. Prockop, D.J. Marrow stromal cells as stem cells for nonhematopoietic tissues. *Science* **276**, 71–74 (1997).
7. Dezawa, M. *et al.* Bone marrow stromal cells generate muscle cells and repair muscle degeneration. *Science* **309**, 314–317 (2005).
8. Mizuno, H. *et al.* Myogenic differentiation by human processed lipoaspirate cells. *Plast. Reconstr. Surg.* **109**, 199–209, Discussion 210–211 (2002).
9. Wakitani, S., Saito, T. & Caplan, A.I. Myogenic cells derived from rat bone marrow mesenchymal stem cells exposed to 5-azacytidine. *Muscle Nerve* **18**, 1417–1426 (1995).
10. Makino, S. *et al.* Cardiomyocytes can be generated from marrow stromal cells *in vitro*. *J. Clin. Invest.* **103**, 697–705 (1999).
11. Rangappa, S., Entwistle, J.W., Wechsler, A.S. & Kresh, J.Y. Cardiomyocyte-mediated contact programs human mesenchymal stem cells to express cardiogenic phenotype. *J. Thorac. Cardiovasc. Surg.* **126**, 124–132 (2003).
12. Oswald, J. *et al.* Mesenchymal stem cells can be differentiated into endothelial cells *in vitro*. *Stem Cells* **22**, 377–384 (2004).
13. Cao, Y. *et al.* Human adipose tissue-derived stem cells differentiate into endothelial cells *in vitro* and improve postnatal neovascularization *in vivo*. *Biochem. Biophys. Res. Commun.* **332**, 370–379 (2005).
14. Dezawa, M. *et al.* Specific induction of neuronal cells from bone marrow stromal cells and application for autologous transplantation. *J. Clin. Invest.* **113**, 1701–1710 (2004).
15. Woodbury, D., Schwarz, E.J., Prockop, D.J. & Black, I.B. Adult rat and human bone marrow stromal cells differentiate into neurons. *J. Neurosci. Res.* **61**, 364–370 (2000).
16. Mimura, T., Dezawa, M., Kanno, H., Sawada, H. & Yamamoto, I. Peripheral nerve regeneration by transplantation of bone marrow stromal cell-derived Schwann cells in adult rats. *J. Neurosurg.* **101**, 806–812 (2004).
17. Dezawa, M., Takahashi, I., Esaki, M., Takano, M. & Sawada, H. Sciatic nerve regeneration in rats induced by transplantation of *in vitro*–differentiated bone-marrow stromal cells. *Eur. J. Neurosci.* **14**, 1771–1776 (2001).
18. Schwartz, R.E. *et al.* Multipotent adult progenitor cells from bone marrow differentiate into functional hepatocyte-like cells. *J. Clin. Invest.* **109**, 1291–1302 (2002).
19. Miyazaki, M. *et al.* Improved conditions to induce hepatocytes from rat bone marrow cells in culture. *Biochem. Biophys. Res. Commun.* **298**, 24–30 (2002).
20. Tang, D.Q. *et al.* *In vivo* and *in vitro* characterization of insulin-producing cells obtained from murine bone marrow. *Diabetes* **53**, 1721–1732 (2004).
21. Timper, K. *et al.* Human adipose tissue-derived mesenchymal stem cells differentiate into insulin, somatostatin, and glucagon expressing cells. *Biochem. Biophys. Res. Commun.* **341**, 1135–1140 (2006).
22. Ferrari, G. *et al.* Muscle regeneration by bone marrow-derived myogenic progenitors. *Science* **279**, 1528–1530 (1998).
23. Orlic, D. *et al.* Bone marrow cells regenerate infarcted myocardium. *Nature* **410**, 701–705 (2001).
24. Lee, J. *et al.* Migration and differentiation of nuclear fluorescence-labeled bone marrow stromal cells after transplantation into cerebral infarct and spinal cord injury in mice. *Neuropathology* **23**, 169–180 (2003).
25. Tomita, M. *et al.* Bone marrow-derived stem cells can differentiate into retinal cells in injured rat retina. *Stem Cells* **20**, 279–283 (2002).
26. Tamai, K. *et al.* PDGFRα-positive cells in bone marrow are mobilized by high mobility group box 1 (HMGB1) to regenerate injured epithelia. *Proc. Natl. Acad. Sci. USA* **108**, 6609–6614 (2011).
27. Sakaida, I. *et al.* Transplantation of bone marrow cells reduces CCl4-induced liver fibrosis in mice. *Hepatology* **40**, 1304–1311 (2004).
28. Zuk, P.A. *et al.* Human adipose tissue is a source of multipotent stem cells. *Mol. Biol. Cell* **13**, 4279–4295 (2002).
29. De Bari, C., Dell'Accio, F., Tylzanowski, P. & Luyten, F.P. Multipotent mesenchymal stem cells from adult human synovial membrane. *Arthritis Rheum.* **44**, 1928–1942 (2001).
30. Ishizeki, K., Nawa, T. & Sugawara, M. Calcification capacity of dental papilla mesenchymal cells transplanted in the isogenic mouse spleen. *Anat. Rec.* **226**, 279–287 (1990).
31. Kim, J.W. *et al.* Mesenchymal progenitor cells in the human umbilical cord. *Ann. Hematol.* **83**, 733–738 (2004).
32. Crigler, L. *et al.* Isolation of a mesenchymal cell population from murine dermis that contains progenitors of multiple cell lineages. *FASEB J.* **21**, 2050–2063 (2007).
33. Fuchs, E. & Segre, J.A. Stem cells: a new lease on life. *Cell* **100**, 143–155 (2000).
34. Hirata, T.M. *et al.* Expression of multiple stem cell markers in dental pulp cells cultured in serum-free media. *J. Endod.* **36**, 1139–1144 (2010).
35. Huang, H.I. *et al.* Multilineage differentiation potential of fibroblast-like stromal cells derived from human skin. *Tissue Eng. Part A* **16**, 1491–1501 (2010).
36. De Bari, C. *et al.* Mesenchymal multipotency of adult human periosteal cells demonstrated by single-cell lineage analysis. *Arthritis Rheum.* **54**, 1209–1221 (2006).
37. Sarugaser, R., Hanoun, L., Keating, A., Stanford, W.L. & Davies, J.E. Human mesenchymal stem cells self-renew and differentiate according to a deterministic hierarchy. *PLoS ONE* **4**, e6498 (2009).
38. Kitada, M. Mesenchymal cell populations: development of the induction systems for Schwann cells and neuronal cells and finding the unique stem cell population. *Anat. Sci. Int.* **87**, 24–44 (2012).
39. Kuroda, Y. *et al.* Unique multipotent cells in adult human mesenchymal cell populations. *Proc. Natl. Acad. Sci. USA* **107**, 8639–8643 (2010).
40. Wakao, S. *et al.* Multilineage-differentiating stress-enduring (Muse) cells are a primary source of induced pluripotent stem cells in human fibroblasts. *Proc. Natl. Acad. Sci. USA* **108**, 9875–9880 (2011).
41. Kucia, M. *et al.* A population of very small embryonic-like (VSEL) CXCR4$^+$SSEA-1$^+$Oct-4$^+$ stem cells identified in adult bone marrow. *Leukemia* **20**, 857–869 (2006).
42. Kucia, M., Wysoczynski, M., Ratajczak, J. & Ratajczak, M.Z. Identification of very small embryonic like (VSEL) stem cells in bone marrow. *Cell Tissue Res.* **331**, 125–134 (2008).
43. D'Ippolito, G. *et al.* Marrow-isolated adult multilineage inducible (MIAMI) cells, a unique population of postnatal young and old human cells with extensive expansion and differentiation potential. *J. Cell Sci.* **117**, 2971–2981 (2004).
44. Toma, J.G., McKenzie, I.A., Bagli, D. & Miller, F.D. Isolation and characterization of multipotent skin-derived precursors from human skin. *Stem Cells* **23**, 727–737 (2005).
45. De Kock, J., Vanhaecke, T., Biernaskie, J., Rogiers, V. & Snykers, S. Characterization and hepatic differentiation of skin-derived precursors from adult foreskin by sequential exposure to hepatogenic cytokines and growth factors reflecting liver development. *Toxicol. In Vitro* **23**, 1522–1527 (2009).
46. Bianco, P., Sacchetti, B. & Riminucci, M. Osteoprogenitors and the hematopoietic microenvironment. *Best Pract. Res. Clin. Haematol.* **24**, 37–47 (2011).
47. Sacchetti, B. *et al.* Self-renewing osteoprogenitors in bone marrow sinusoids can organize a hematopoietic microenvironment. *Cell* **131**, 324–336 (2007).

ヒト生体に内在する新たな多能性幹細胞　Muse細胞：細胞治療，予後の診断，創薬，病態解析への展開の可能性

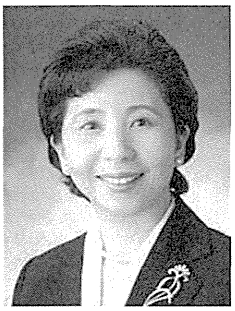

東北大学大学院医学系研究科細胞組織学分野・人体構造学分野
出澤 真理
Mari DEZAWA

1.　はじめに

間葉系幹細胞は骨髄，脂肪，真皮，臍帯などに存在する組織幹細胞であり，腫瘍化の危険が低く安全性が高いこと，入手しやすい組織から得られることなどから，臨床試験が各国で精力的に進められている。栄養因子やサイトカインの産生による組織保護効果や抗炎症作用，アポトーシス調節作用をもたらすので様々な疾患を対象に移植が検討されており，また免疫抑制作用も持つことから，移植片対宿主病に対する臨床応用も進められている。

しかし，間葉系幹細胞にはこれらの作用の他に重要な作用がある。それは，胚葉を超えた幅広い分化と生体内での組織修復作用である。これらの作用は長らく科学的に議論されてきたが，間葉系幹細胞が様々な細胞種の混合から成り立っており，そのような幹細胞の本態が明らかにされてこなかったことや，生体内での組織修復効果の率が極めて低いなどの理由から実態がよくわかっていなかった。

我々の研究室ではヒトの間葉系組織や間葉系の培養細胞において，多能性を有するが腫瘍性を持たない新たなタイプの体性幹細胞Multiliniage-differentiating stress enduring (Muse) 細胞を見出した[1),2)]。この細胞は，成人の生体内に存在する多能性幹細胞であり，これまで間葉系幹細胞で見られてきた幅広い分化能や組織修復を説明すると考えられる。

■ 著者連絡先
東北大学大学院医学系研究科細胞組織学分野・人体構造学分野
（〒980-8575　宮城県仙台市青葉区星陵町2-1）
E-mail. mdezawa@med.tohoku.ac.jp

2.　生体内多能性幹細胞としてのMuse細胞

Muse細胞は間葉系幹細胞の一員であると同時に，多能性幹細胞としての振る舞いを見せる。このような特性はマーカーの発現にも見られ，間葉系マーカーCD29，CD105，CD90と同時に，未分化ヒトES細胞のマーカーstage specific embryonic antigen-3 (SSEA-3) のダブル陽性細胞，すなわち間葉系と多能性幹細胞の両方のマーカーを発現する細胞として同定される。

Muse細胞は1細胞レベルでの浮遊培養を行うと増殖を開始し，ヒトES細胞由来の胚葉体と酷似した細胞塊clusterを形成する[1)]。このclusterはアルカリフォスファターゼ反応に陽性を示し，Nanog，Sox2，Oct3/4などの多能性マーカーを発現する。さらに，この1細胞から形成された細胞塊をゲラチン上で培養するとsmooth muscle actin（平滑筋），desmin（骨格筋），alpha-fetoprotein（肝細胞），cytokeratin-7（胆道系細胞），neurofilament（神経）など三胚葉性の細胞へ自発的に分化する[1)]。このような自発的な三胚葉性の細胞への分化率は高くはなく，内胚葉性や外胚葉性の細胞が全体の3～4%，中胚葉性の細胞が10～15%であるが，一方，Muse細胞に特定の誘導をかけると90%以上の高い効率で神経，肝細胞，脂肪細胞，骨細胞などの目的とする細胞に分化させることが可能である。従ってMuse細胞からは効率の良いdirect reprogrammingが可能である。

Muse細胞は成人ヒトの皮膚，骨髄などの間葉系組織から採取可能である。生体の間葉系組織の場合，例えば骨髄液では，3,000個の骨髄単核球細胞のうち1細胞の割合で存在する[1),2)]。生体内でのMuse細胞の局在を組織学的に検討すると，真皮，脂肪組織や他の様々な臓器では結合組織内に孤立性・散在性に存在し，特定の組織構造との関連は

見られなかった[2]。また，市販の間葉系の培養細胞では，多少の増減はあるものの大体1%ないし数%程度の割合で含まれている。

3. Muse細胞は多能性であるが腫瘍性がない

腫瘍性増殖能に関わる因子の発現量を調べるとembryonic stem (ES) 細胞，induced pluripotent stem (iPS) 細胞は非常に高値を示すが，Muse細胞では体細胞とほぼ同じレベルで低い[2]。さらにヒト細胞への免疫拒絶を示さない免疫欠損マウス（SCIDマウス）の精巣への移植では，ヒトES細胞やiPS細胞は8～12週で奇形腫を形成するのに対し，ヒトMuse細胞では半年を経過しても奇形腫の形成は全く見られなかった[1]。間葉系幹細胞は腫瘍化の危険が低く，すでにヒトに移植されている細胞であり，Muse細胞はその間葉系幹細胞の一部であることと併せて考えると，もともと腫瘍化の危険は低いと思われる。

4. Muse細胞は生体に投与されると組織修復機能をもたらす

ヒト細胞を拒絶しない免疫欠損マウスを用いて劇症肝炎，筋変性，脊髄損傷，皮膚損傷などの様々なモデルを作製し，GFPで標識したヒトMuse細胞を尾静脈から投与すると（ただし皮膚損傷の場合は局所注入を行った），移植4週後でMuse細胞は傷害部位に生着し，肝細胞，筋細胞，神経細胞，角化細胞にそれぞれ分化することが確認されている[1]。

SCIDマウスの腹腔に四塩化炭素を投与して作製した劇症肝炎モデルでは，尾静脈から投与したGFP陽性のヒトMuse細胞が肝臓の傷害部位に経血管的に生着しており，さらに，生着した細胞の約90%近くがヒトアルブミンやヒトアンチトリプシンをマウス肝臓内発現することが確認された。マウスの末梢血を採取しWestern blotで解析するとヒトアルブミンが検出されたことから，移植されたヒトのMuse細胞がマウスの肝臓内に生着し，ヒト肝細胞として分化し，さらにヒトのアルブミンを血中に放出することのできる機能的細胞になっていたということを示唆する[1]。

同様に，筋変性モデルに生着したヒトMuse細胞はヒトのジストロフィンを，損傷脊髄ではneurofilamentを，損傷皮膚ではcytokeratin 14を発現していた[1]。このように，投与されたヒトMuse細胞は生体内で損傷部位を認識して生着し，機能的な細胞に分化すること，さらに三胚葉性の細胞に生体内でそれぞれ分化することが示された。

一方Muse細胞を除いたヒト間葉系幹細胞，すなわち非Muse細胞群を同様の方法で生体に投与しても，Muse細胞で見られたような損傷組織への生着や各組織の細胞への分化は観察されない[1]。従って，Muse細胞は損傷部位を認識し，組織を構成する細胞となりうる組織修復機能を持つが，Muse細胞以外の間葉系幹細胞にはこのような機能が備わっていない，すなわち間葉系幹細胞移植においてこれまで見られてきた組織再生，組織修復はMuse細胞が担っていると考えられる。

Muse細胞の特性をまとめると，

- 遺伝子導入などの人工的な操作なしに，ヒト生体から直接得られる多能性幹細胞。三胚葉性の多様な細胞に分化できる。
- 入手しやすい皮膚，骨髄，脂肪や市販の線維芽細胞などから採取可能である。
- 腫瘍化の危険性が低い。
- 骨髄移植の0.03%，間葉系幹細胞移植の数%に相当。すでに移植されている細胞の一部であり，安全性の見通しが高い。
- 培養では線維芽細胞と同程度の増殖力を持ち，脂肪や骨髄から細胞数確保が可能。
- 生体内にそのまま投与すると組織修復をもたらす。

などの特徴に集約される。

5. 再生医療におけるMuse細胞の可能性と戦略

間葉系幹細胞は組織保護や修復に効果があるとされ，臨床応用も進められているが，特に再生効果・組織修復作用に関しては明快な科学的根拠が提示されてこなかった。そのような中で，三胚葉性の細胞への幅広い分化能力を有する多能性のMuse細胞が間葉系幹細胞の中から同定され，さらにはこの細胞が再生効果，組織修復効果を担っているということが明らかになったことには再生医学において意義がある。これまで雑駁な間葉系幹細胞をそのまま生体に投与する形で臨床試験などが行われているが，その中に含まれるMuse細胞を精製する，あるいは比率を上げることによって組織修復効率の向上や有効性の高い再生医療への応用が期待される。ただし，Muse細胞以外の間葉系細胞が必要であるのか不要なのか，この点は慎重な判断が必要と思われる。疾患によっては急性の炎症，組織破壊など複合的な要因が絡み合っている場合がある。このような「場」にMuse細胞だけを投与するよりも，抗炎症，抗アポトーシス作用を持ち組織保護をもたらす非Muse細胞が一定程度存在するほうが，Muse細胞自身の生着，生存が上がり，結果として有効な組織再生につながる可能性がある。Muse細胞をどのように有効活用するかは今後の大きな課題である。

本稿の著者には規定されたCOIはない。

文　献

1) Kuroda Y, Kitada M, Wakao S, et al: Unique multipotent cells in adult human mesenchymal cell populations. Proc Natl Acad Sci USA **107**: 8639-43, 2010
2) Wakao S, Kitada M, Kuroda Y, et al: Multilineage-differentiating stress-enduring (Muse) cells are a primary source of induced pluripotent stem cells in human fibroblasts. Proc Natl Acad Sci USA **108**: 9875-80, 2011

Research article

Autologous mesenchymal stem cell–derived dopaminergic neurons function in parkinsonian macaques

Takuya Hayashi,[1,2,3,4] Shohei Wakao,[5] Masaaki Kitada,[5] Takayuki Ose,[1] Hiroshi Watabe,[1,6] Yasumasa Kuroda,[7] Kanae Mitsunaga,[5] Dai Matsuse,[5] Taeko Shigemoto,[5] Akihito Ito,[8] Hironobu Ikeda,[8] Hidenao Fukuyama,[3] Hirotaka Onoe,[1] Yasuhiko Tabata,[9] and Mari Dezawa[5,7]

[1]Functional Probe Research Laboratory, Center for Molecular Imaging Science, RIKEN, Kobe, Japan. [2]National Cerebral Cardiovascular Center Research Institute, Osaka, Japan. [3]Human Brain Research Center, Graduate School of Medicine, and [4]Center for iPS Cell Research and Application, Kyoto University, Kyoto, Japan. [5]Department of Stem Cell Biology and Histology, Tohoku University Graduate School of Medicine, Sendai, Miyagi, Japan. [6]Faculty of Molecular Imaging in Medicine, Osaka University Graduate School of Medicine, Suita, Osaka, Japan. [7]Department of Anatomy and Anthropology, Tohoku University Graduate School of Medicine, Sendai, Miyagi, Japan. [8]Shiga Research Institute, Nissei Bilis Co. Ltd., Koga, Shiga, Japan. [9]Department of Biomaterials, Field of Tissue Engineering, Institute for Frontier Medical Sciences, Kyoto University, Kyoto, Japan.

A cell-based therapy for the replacement of dopaminergic neurons has been a long-term goal in Parkinson's disease research. Here, we show that autologous engraftment of A9 dopaminergic neuron-like cells induced from mesenchymal stem cells (MSCs) leads to long-term survival of the cells and restoration of motor function in hemiparkinsonian macaques. Differentiated MSCs expressed markers of A9 dopaminergic neurons and released dopamine after depolarization in vitro. The differentiated autologous cells were engrafted in the affected portion of the striatum. Animals that received transplants showed modest and gradual improvements in motor behaviors. Positron emission tomography (PET) using [^{11}C]-CFT, a ligand for the dopamine transporter (DAT), revealed a dramatic increase in DAT expression, with a subsequent exponential decline over a period of 7 months. Kinetic analysis of the PET findings revealed that DAT expression remained above baseline levels for over 7 months. Immunohistochemical evaluations at 9 months consistently demonstrated the existence of cells positive for DAT and other A9 dopaminergic neuron markers in the engrafted striatum. These data suggest that transplantation of differentiated autologous MSCs may represent a safe and effective cell therapy for Parkinson's disease.

Introduction

Cell-based therapies are expected to replace the missing dopaminergic neurons and to restore the motor function in patients with Parkinson's disease (PD) (1). Early studies on cell-based therapies used fetal midbrain tissue containing dopaminergic neurons as a cell source and suggested potential therapeutic effects in PD (for review, see refs. 2, 3). However, limited availability and ethical considerations relating to the use of fetuses pose limitations for practical use. Bone marrow–derived mesenchymal stem cells (MSCs), a type of adult stem cells, have trophic effects (4) and a differentiation spectrum that crosses oligolineage boundaries (5), offering the potential for use in autologous cell therapy, with low risk of tumorigenesis (6). The MSCs have been already tested for cell therapy in PD model rodents (7–9) and even in patients with PD (10). However, they have shown poor performance for restoration of motor function, potentially due to limited spontaneous differentiation (11) or facilitated apoptosis (12, 13) of MSCs. Recent studies of fetal midbrain graft have suggested that better outcomes could be obtained if the graft consisted of well-differentiated A9 dopaminergic neurons (14–16), the most severely damaged neuronal type in PD (17). Therefore, differentiation of MSCs into desired cells, such as A9 dopaminergic neurons, would probably provide effective functional restoration in PD.

Recently, it was shown that MSCs could be artificially directed to differentiate into several specialized cell types, including those in nervous tissues (18–21). Previously, we reported that dopamine-producing cells could be induced from MSCs (MSC-DP cells) by introduction of a Notch1 intracellular domain–containing (NICD-containing) plasmid, followed by cytokine stimulation with bFGF, forskolin, ciliary neurotrophic factor (CNTF), and glial cell line–derived neurotrophic factor (GDNF) (20, 21). The differentiated cells were positive for markers of dopaminergic neurons, such as tyrosine hydroxylase (TH) and the dopamine transporter (DAT), and had an ability to release dopamine after depolarization by potassium stimulation. When rat and human MSC-DP cells were transplanted into the striata of PD model rats, integration of TH$^+$ and DAT$^+$ cells and functional recovery in motor behaviors were confirmed (20). Subsequent development of a spermine-pullulan–mediated reverse transfection method allowed us to induce MSC-DP cells more safely and efficiently than before from MSCs of macaque monkeys (21), an animal species frequently used for preclinical trials of PD (22–27).

To test the scalability of MSC-DP cell–based therapy in primates in this study, monkey MSC-DP cells were characterized in detail using specific markers and evaluated for their longitudinal effects after they were engrafted into hemiparkinsonian monkeys using behavioral tests and positron emission tomography (PET). The MSC-DP cells, prepared autologously from the bone marrow of

Authorship note: Takuya Hayashi and Shohei Wakao contributed equally to this work.

Conflict of interest: The authors have declared that no conflict of interest exists.

Citation for this article: *J Clin Invest.* doi:10.1172/JCI62516.

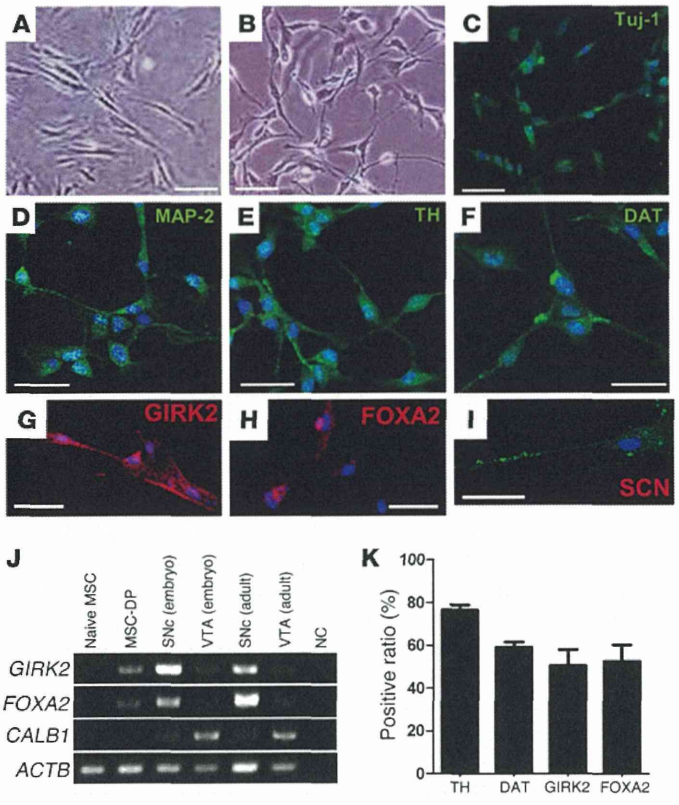

Figure 1

Monkey bone marrow MSCs and MSC-DP cells. (**A**) Morphological changes were evident in cynomolgus naive MSCs (phase-contrast microscopy) and (**B**) MSC-DP cells (phase-contrast microscopy). The MSC-DP cells possessed neurite-like processes. Immunocytochemistry of MSC-DP cells showed that the cells were immunoreactive for the neuronal markers (**C**) Tuj1 and (**D**) MAP-2; for the markers of dopaminergic neurons (**E**) TH, (**F**) DAT, (**G**) GIRK2, and (**H**) FOXA2; and for the marker of neurons, (**I**) sodium channel (SCN). DAPI was used for counterstaining of nuclei. Scale bar: 30 μm. (**J**) Results of RT-PCR in naive MSCs, MSC-DP cells, and tissue samples from the SNc and VTA. Naive MSCs expressed no *GIRK2*, *FOXA2*, and *CALB1* mRNA, while the MSC-DP cells expressed *GIRK2* and *FOXA2* mRNA. SNc tissue samples from an embryo and an adult cynomolgus monkey also contained high levels of *GIRK2* and *FOXA2* mRNA but only low levels of *CALB1* mRNA, while the VTA contained high levels of *CALB1* mRNA and only very low levels of *GIRK2* and *FOXA2* mRNA. NC, negative control. (**K**) Percentages of cells immunoreactive for TH, DAT, GIRK2, and FOXA2 in MSC-DP cells.

each test animal, expressed cell makers not only for antigens that have been previously described (20, 21), such as β tubulin III (Tuj1), microtubule-associated protein 2 (MAP-2), TH, and DAT, but also for those specific to the A9 subtype, namely, G protein–coupled inward rectifying current potassium channel type 2 (GIRK2) (15) and forkhead box protein A2 (FOXA2) (28). The effect of transplantation was evaluated for up to 9 months based on motor behaviors of affected hand movements; PET scans using ^{11}C-CFT, which specifically labels DAT; and postmortem histology. Tumorigenicity was also estimated from the results of blood tests and PET scans. The preclinical data obtained thus may extend the applicability of the current autologous cell system as a therapy for PD.

Results

Evaluation of MSC-DP cells. Cynomolgus monkey MSCs drastically changed their morphology following induction, as reported previously (21): naive MSCs initially showed fibroblast-like mesenchymal cell features (Figure 1A), while induced cells showed a neuron-like morphology with neurite-like processes (Figure 1B). By immunohistochemistry, naive MSCs were negative for neuronal markers, as reported previously (21), but induced cells were positive for neuronal markers, Tuj1 (Figure 1C) and MAP-2 (Figure 1D); dopaminergic neuron markers, TH and DAT (Figure 1, E and F); the A9 dopaminergic neuron marker, GIRK2 (Figure 1G); and a marker of floor plate–derived cells, FOXA2 (Figure 1H). We also confirmed that these cells were positive for sodium channels (Figure 1I), a marker of differentiated neurons.

To confirm whether these cells have an ability to produce and release dopamine, we measured the secretion of dopamine by HPLC. The amount of dopamine in the culture supernatant was measured following application of high K^+ depolarizing stimuli, which resulted in release of 1.04 ± 0.4 pM dopamine per 10^6 cells (Table 1); by contrast, naive cynomolgus monkey MSCs showed no detectable dopamine release. These results are consistent with those of our previous studies: the amount of dopamine release was comparable to the amounts in rats (1.1 pM/10^6 cells) (20) and monkeys (0.9 ± 0.2 pM/10^6 cells) (21).

We further investigated the expression of markers specific for A9 dopamine neurons using RT-PCR. The MSC-DP cells expressed *GIRK2* and *FOXA2* mRNA but not *CALB1* mRNA (*GIRK2*$^+$/*FOXA2*$^+$/*CALB1*$^-$) (Figure 1J). When control tissues obtained from a cynomolgus embryo and an adult animal were analyzed, both showed that the substantia nigra pars compacta (SNc) was strongly positive for GIRK2 and FOXA2 and weakly positive for calbindin, while the ventral tegmental area (VTA) was weakly positive for GIRK2 and FOXA2 but strongly positive for calbindin (Figure 1J). This distinct pattern of GIRK2/FOXA2/calbindin expression in the SNc and VTA is consistent with those reported in other species, including rodents and humans (15, 28, 29). We also evaluated the induction efficiency of MSC-DP cells by quantitative immunocytochemistry. Fifty to seventy-five percent of MSC-DP cells were positive for TH, DAT, GIRK2, and FOXA2 (Figure 1K). These findings indicated that the current method efficiently produced MSC-DP cells from the MSCs, which had properties similar to those of the A9 dopamine neurons in the model species.

Behavioral analysis of motor symptoms. The clinical rating scores (CRSs) for parkinsonian animals are shown in Figure 2A. The CRS revealed a significant interaction effect between groups and time

Table 1
Dopamine-producing capacity of MSC-DP cells and the number of engrafted cells

Animal ID	Dopamine release induced by K^+ (pM/10^6 cells)	No. of engrafted cells (× 10^6 counts)
mon0703	2.6	20.4
mon0705	0.5	9.0
mon0708	0.4	12.0
mon0709	0.8	12.7
mon0710	0.9	18.6

Dopamine release induced by K^+ was measured by HPLC. Animals were from the MSC-DP–engrafted group.

after transplantation (F distribution [$F_{4,32}$] = 3.07, $P < 0.05$). Thus, we further tested for an effect of time, separately in each of the groups in our study (engrafted or sham), by 1-way ANOVA. The CRS in the MSC-DP–engrafted group showed a marginal effect of time ($F_{4,16} = 2.95$, $P = 0.055$). In a post-hoc comparison of scores at each time point after engraftment with those at baseline, significant improvements in the CRS were observed at 8 months after engraftment (Dunnett's multiple comparison, $P < 0.05$). This time effect was not observed in the sham group either by 1-way ANOVA or post-hoc analysis.

Hand-reach scores showed similar time courses (Figure 2B). The scores for the affected hand showed significant group and time interaction ($F_{4,32} = 2.83$, $P < 0.05$). One-way ANOVA for the repeated measures of hand-reach scores for the affected hand of the MSC-DP–engrafted group revealed a significant effect of time ($F_{4,16} = 5.62$, $P < 0.001$). A post-hoc comparison of scores at each time point after engraftment with those at baseline revealed significant improvements in hand-reach scores at 4 months (Dunnett's multiple comparison, $P < 0.05$) and 8 months ($P < 0.01$) after engraftment. This effect of time was not observed in the sham group. Therefore, the CRSs and hand-reach scores suggested that the engraftment of MSC-DP cells modestly improved motor behaviors in parkinsonian animals.

Despite these improvements in MSC-DP–grafted animals, spontaneous activities of animals were not affected by any of group (sham vs. MSC-DP engrafted), time (before engraftment and 4 months and 8 months after engraftment), or interaction among these variables (2-way ANOVA with repeated measures, Supplemental Figure 1; supplemental material available online with this article; doi:10.1172/JCI62516DS1). Animals in the engrafted group tended to show higher spontaneous activities than sham-operated animals at 4 and 8 months after engraftment; however, no statistically significant effect of group was observed at any time point in post-hoc analysis (Bonferroni corrected, $P > 0.05$). Within-subject and between-subject data were highly variable, consistent with a previous report in this type of parkinsonian animal model (30). No dyskinesia-like abnormal movements were observed in any MSC-DP cell–engrafted animals during the observation period.

^{11}C-CFT PET. Voxel-based analysis of ^{11}C-CFT binding potential (BP_{ND}) images disclosed a significant effect of time in a cluster extending into the dorsal posterior putamen in the engrafted group (Figure 3C) (family-wise error rate [FWE] corrected, $P < 0.05$; Table 2). The maximum of this cluster was located ($x = 11.5$ mm, $y = -8.0$ mm, $z = 3.5$ mm) in a standard macaque brain space of the Montreal Neurological Institute (MNI) (31) and was safely within the area targeted when engrafting MSC-DP cells into the striatum (Figure 3A). Using this cluster as a region of interest (ROI), we obtained BP_{ND} values for this ROI across all animals, groups, and time points. The BP_{ND} values obtained are presented in Figure 3D. Two-way ANOVA with repeated measures (Figure 3D) revealed significant effects of an interaction between group and time ($F_{4,24} = 4.3$, $P < 0.01$). Post-hoc analysis showed that the BP_{ND} at 7 days after engraftment was higher than that in the sham-operated group (Bonferroni multiple comparison, $T = 4.56$, $P < 0.001$), as shown in Figure 3D. In particular, animal mon0703, who received the graft with the largest amount of MSC-DP cells (Table 1), showed the highest BP_{ND} (0.59) in the engrafted striatum at 7 days after engraftment, followed by animal mon0710, who showed a BP_{ND} of 0.43 at 7 days after engraftment (Figure 3B).

The time-dependent decline in ^{11}C-CFT binding in the engrafted striatum (Figure 3D) allowed us to analyze the kinetics of ^{11}C-CFT binding in detail. Because recent studies have suggested that MSCs are susceptible to senescent (12) and apoptotic changes (13), we supposed that this decline was due to degeneration of engrafted MSC-DP cells. ^{11}C-CFT binding is known to be correlated with the density of dopamine neurons or terminals rather than any physiological (or functional) variation in dopamine release. The rate of ^{11}C-CFT binding reduction, calculated based on the 1-hit model of neurodegeneration (32), was 0.30 months (~10 days) as a half-life period (Figure 3E). This rate of reduction was slightly slower than that for engrafted naive rodent MSCs (~3 days; Supplemental Figure 2) based on previously described data (13). We further tested whether this degenerative process would affect all grafted cells. The plateau of the 1-hit model was significantly higher than the baseline (before engraftment) ^{11}CFT binding level (baseline $BP_{ND} = 0.087 \pm 0.028$ vs. BP_{ND} at plateau = 0.17 ± 0.029; Welch's corrected $T_{13} = 2.04$, 1-tailed $P < 0.05$), suggesting that a small portion of the grafted MSC-DP cells survive and integrate

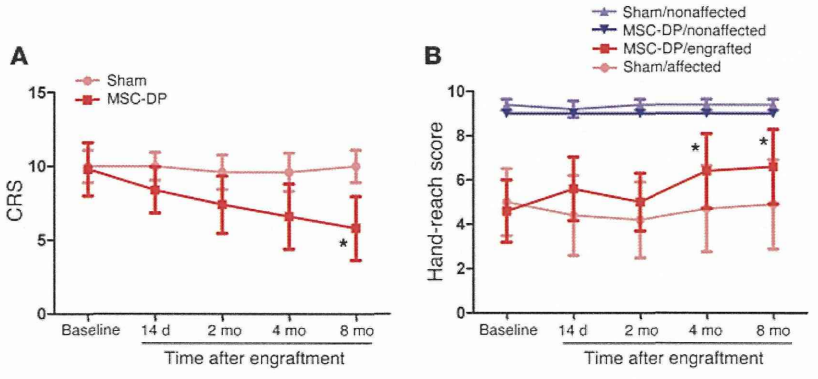

Figure 2
Behavioral assessment. (**A**) CRSs and (**B**) hand-reach scores were plotted against time for MSC-DP cell–engrafted (MSC-DP) and sham-operated (Sham) groups. *$P < 0.05$ compared with baseline in the MSC-DP–engrafted group, Dunnett's multiple comparison test.